

See discussions, stats, and author profiles for this publication at: <https://www.researchgate.net/publication/262317738>

# Surface Properties of Encapsulating Hydrophobic Nanoparticles Regulates the Main Phase Transition Temperature of Lipid Bilayers: A Simulation Study

ARTICLE *in* NANO RESEARCH · APRIL 2014

Impact Factor: 7.01 · DOI: 10.1007/s12274-014-0482-3

---

CITATIONS

3

---

READS

42

## 2 AUTHORS:



Xubo Lin

University of Texas Health Science Center at ...

12 PUBLICATIONS 77 CITATIONS

[SEE PROFILE](#)



Gu Ning

Southeast University (China)

419 PUBLICATIONS 6,795 CITATIONS

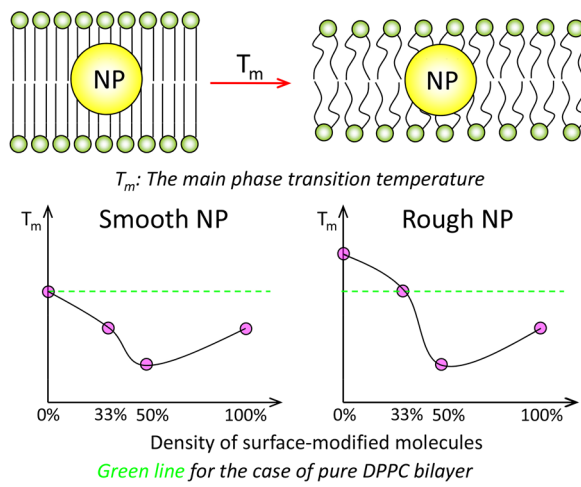
[SEE PROFILE](#)

## TABLE OF CONTENTS (TOC)

### Surface Properties of Encapsulating Hydrophobic Nanoparticles Regulates the Main Phase Transition Temperature of Lipid Bilayers: A Simulation Study

Xubo Lin, Ning Gu\*

State Key Laboratory of Bioelectronics and Jiangsu Key Laboratory for Biomaterials and Devices, School of Biological Science & Medical Engineering, Southeast University, Nanjing, 210096, People's Republic of China



The main phase transition temperature of lipid bilayers can be regulated by changing the surface roughness and surface molecule density of encapsulating hydrophobic nanoparticles, which may promote potential biomedical applications such as controllable drug release.

Provide the authors' website if possible.

Prof. Ning Gu, <http://lbmd.seu.edu.cn/nano/>

# Surface Properties of Encapsulating Hydrophobic Nanoparticles Regulates the Main Phase Transition Temperature of Lipid Bilayers: A Simulation Study

Xubo Lin, Ning Gu (✉)

State Key Laboratory of Bioelectronics and Jiangsu Key Laboratory for Biomaterials and Devices, School of Biological Science & Medical Engineering, Southeast University, Nanjing, 210096, People's Republic of China

Received:

Revised:

Accepted:

© Tsinghua University Press  
and Springer-Verlag Berlin  
Heidelberg 2014

## KEYWORDS

lipid bilayer,  
phase transition,  
nanoparticle,  
surface roughness,  
density,  
surface molecules

## ABSTRACT

The main phase transition temperature of a lipid membrane, which is vital for its biomedical applications such as controllable drug release, can be regulated by encapsulating hydrophobic nanoparticles into the membrane. However, the exact relationship between surface properties of encapsulating nanoparticles and the main phase transition temperature of lipid membrane is far from clear. In the present work, we performed coarse-grained molecular dynamics simulations to meet this end. The results show the surface roughness of nanoparticles and the density of surface-modified molecules of nanoparticles should be responsible for the regulation. Increasing surface roughness of nanoparticles could increase the main phase transition temperature of the lipid membrane, which can be decreased in a nonlinear way via increasing the density of surface-modified molecules of nanoparticles. The results may provide insights for understanding recent experimental studies and promote the applications of nanoparticles in controllable drug release by regulating the main phase transition temperature of lipid vesicles.

## 1 Introduction

Hybrid lipid vesicle-hydrophobic nanoparticle (NP) systems have attracted broad interests based on their advantages in diagnostic and therapeutic applications.<sup>1</sup> NPs can stabilize the lipid vesicle,<sup>2</sup> modulate the phase behavior of the lipid vesicle,<sup>3, 4</sup> trigger the lipid vesicle to release its inclusions under the external field for controlled drug release,<sup>5-7</sup> and so on. Besides, lipids may improve the biocompatibility

of NPs, which promotes the biomedical applications of hydrophobic NPs such as medical imaging,<sup>8, 9</sup> etc.

The synthesis of hybrid lipid vesicle-hydrophobic NP systems has received extensive researches. Theoretically, neutral hydrophobic NPs of size less than or comparable to the membrane thickness can be easily encapsulated into the bilayer of the lipid vesicle.<sup>10-12</sup> Besides, shape also affects the efficiency of encapsulation.<sup>13, 14</sup> Experimentally, for one thing, the encapsulation of certain NPs can be achieved by

Address correspondence to Prof. Ning Gu ([guning@seu.edu.cn](mailto:guning@seu.edu.cn))

modifying proper molecules to the surface of NPs.<sup>15</sup> For another, synthesizing inorganic NPs of specific size, shape, surface chemistry has already become possible,<sup>16-19</sup> which ensures the success of the encapsulation. For example, Rasch *et al.*<sup>20, 21</sup> coated dodecanethiol Au NPs (diameter less than 2nm), mixed the products with lipids, and successfully obtained hybrid systems using self-assembly method. Lee *et al.*<sup>22</sup> fractionized NPs with hydrophobic and hydrophilic ligands and realized the incorporation of NPs with size greatly exceeding the bilayer thickness.

Since NPs of various properties can be incorporated into the lipid bilayer, many further researches focus on the effects of NPs on the lipid bilayer. Park *et al.*<sup>23</sup> entrapped Ag NPs into the hydrophobic region of dipalmitoylphosphatidyl-choline (DPPC) liposomes and found Ag NPs can increase membrane fluidities above the main phase transition temperature of DPPC molecules (41°C). They further found Au NPs have the similar effects.<sup>24</sup> Bothun *et al.* embedded Ag-decanethiol NPs into the bilayer and demonstrated increasing nanoparticle concentration could suppress the lipid pre-transition temperature, reduce the main phase transition temperature, and disrupt gel phase bilayers using differential scanning calorimetry and fluorescence anisotropy.<sup>25</sup> Recently, they further found that high loading of embedding stearylamine (SA)-stabilized Au NP induced large increases in the main phase transition temperature of DPPC/DPPG vesicles.<sup>26</sup> They ascribed this behavior to the cooperative effects of excess free SA ligands and NPs. Here comes out a very charming experimental phenomenon that the main phase transition temperature of the lipid bilayer can be either reduced or increased by encapsulating NPs of certain surface properties. However, the precise relationship between surface properties of NPs and changes of the main phase transition temperature is far from being fully understood, which is the focus of this work.

The main phase transition process (gel-to-fluid phase transition) is primarily a cooperative rotameric disordering of the hydrocarbon chains, which is determined by combined excluded volume interactions and attractive van der Waals interchain interactions.<sup>27</sup> Both these two main interactions can both be properly reproduced using Martini force field.<sup>28</sup> Hence, it is proper to use Martini force field to

study the main phase transition of lipid membrane. Several recent simulation studies have validated the applicability of Martini force field to study phase transition process of lipid membrane.<sup>29-33</sup> It is worth mentioning that the size of the lipid vesicle for the hybrid NP-vesicle system generally exceeds hundreds of nanometers in diameter and the small local region of the hybrid system can be approximated as a planar lipid bilayer (about tens of nanometers scale) encapsulating hydrophobic NPs. Therefore, in this study, we focus on the effects of surface chemistry such as surface roughness and surface ligand density of hydrophobic NPs on changes of the main phase transition temperature of planar lipid bilayer.

## 2 Model and simulation details

Briefly, Martini CG model is based on a four-to-one mapping, i.e., on average four heavy atoms are represented by a single interaction site. Only four main types of interaction sites are defined: polar (P), nonpolar (N), apolar (C), and charged (Q). Each particle type has a number of subtypes, which allow for a more accurate representation of the chemical nature of the underlying atomic structure. Within a main type, subtypes are either distinguished by a letter denoting the hydrogen-bonding capabilities (d donor, a acceptor, da both, 0 none), or by a number indicating the degree of polarity (from 1, low polarity, to 5, high polarity). A shifted Lennard-Jones (LJ) 12-6 potential energy function  $U_{LJ}(r) = 4\epsilon_{ij}\left[\left(\frac{\sigma_{ij}}{r}\right)^{12} - \left(\frac{\sigma_{ij}}{r}\right)^6\right]$  ( $\sigma_{ij}$  representing the closest distance of approach between two particles and  $\epsilon_{ij}$  the strength of their interactions) and a shifted Coulombic potential energy function  $U_{el}(r) = \frac{q_i q_j}{4\pi\epsilon_0\epsilon_r r}$  (relative dielectric constant  $\epsilon_r = 15$  for explicit screening) are used to describe the non-bonded interactions. A weak harmonic potential  $V_{bond}(R) = \frac{1}{2}K_{bond}(R - R_{bond})^2$  (an equilibrium distance  $R_{bond} = \sigma = 0.47\text{ nm}$  and a force constant of  $K_{bond} = 1250\text{ kJ} \cdot \text{mol}^{-1} \cdot \text{nm}^{-2}$ ) is applied for the bonded interactions. A weak harmonic potential  $V_{angle}(\theta) = \frac{1}{2}K_{angle}\{\cos(\theta) - \cos(\theta_0)\}^2$  is used for the angles to represent chain stiffness. For aliphatic chains, the force constant  $K_{angle} = 25\text{ kJ} \cdot \text{mol}^{-1}$  and the

equilibrium bond angle  $\theta_0 = 180^\circ$ ; for the cis double bond,  $K_{angle} = 35 \text{ kJ} \cdot \text{mol}^{-1}$  and  $\theta_0 = 120^\circ$ . More details can be found in Electronic Supplementary Material or in the paper of Marrink *et al.*<sup>28</sup>

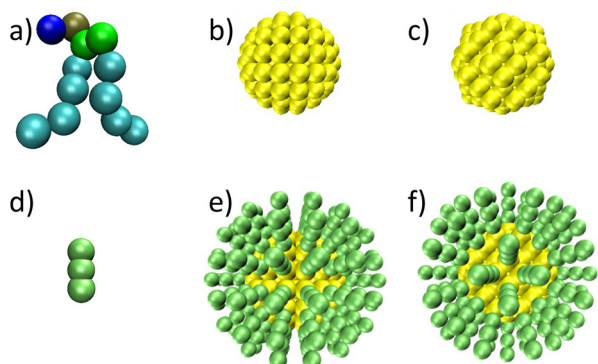


Figure 1. Snapshots of coarse-grained DPPC molecule (a), smooth NP (b), rough NP (c), ligand molecule (d), smooth NP with ligand molecules (e), rough NP with ligand molecules (f). The CG beads of NP (yellow) and ligand molecule (lime) have the same hydrophobic properties as that of DPPC tail (cyan).

Considering that the size of the lipid vesicle for the hybrid NP-vesicle system generally exceeds hundreds of nanometers in diameter, the small local region of the hybrid system can be approximated as a planar lipid bilayer encapsulating hydrophobic NPs. In this study, our systems each include a planar DPPC bilayer of 512 DPPC molecules, 17920 CG waters, and a NP. The CG representations of DPPC and water molecules are the same as in the references.<sup>28</sup> In this work, we focus on physical surface properties, such as surface roughness and surface molecule density, rather than surface chemistry of NP. Hence, we choose C1-type bead, which is the same as the tails of DPPC molecules, to build hydrophobic NPs and ligand molecules. Beads are placed evenly on the concentric spherical surfaces to obtain surface smooth NP (Figure 1b); beads are stacked in face-centered cubic (FCC) way to form surface rough NP (Figure 1c), and all beads of NP within 1nm are constrained by a bond to confirm a rigid NP. Here, this modeling method of the nonspecific NP has been widely used using Martini and other coarse-grained models,<sup>11, 34-44</sup> which helps elucidating the general effects of NP's properties (such as size, shape, surface chemistry, stiffness, etc.) on its interactions with lipid bilayer. As for the ligand molecule, we choose three-bead model, the length of

which is close to that of 12-carbon straight-chain alkanes. 0%, 33%, 50%, 100% of surface beads of NPs (diameter, d=3nm) are evenly modified with ligand molecules to realize different ligand density on the surface. Besides, NPs (d=4nm) is also considered as a control group to evaluate the effects of size increase induced by surface ligands.

Hydrophobic NP was firstly placed in the water near the DPPC bilayer (The minimal distance between NP and the bilayer is 0.5nm.) and the system was relaxed for 200ns at temperature of T=335K. Then, an external force was exerted on NP to drag it into the hydrophobic region of the DPPC bilayer. (The dynamic of NPs penetrating into the lipid bilayer has been widely probed. Hence, we use an external force just to obtain the conformation of lipid bilayer with the encapsulation of NP.) All NPs can be easily embedded in the DPPC bilayer to form the stable hybrid systems. The hybrid system was cooled by  $\Delta T=5\text{K}$  step by step until 280K. The output configuration at T was used as starting input for the system at  $T-\Delta T$  and a 400ns equilibrium run was performed at each temperature with last 100ns for data analysis (At each temperature, the system can reach the equilibrium within 300ns.). The final conformation at T=280K was used as the initial state for gel-to-fluid phase transition simulation (heating process), which had a similar procedure as mentioned above but in a reverse direction.

For all simulations, a cutoff of 1.2 nm was used for van der Waals (vdW) interactions, and the Lennard-Jones potential was smoothly shifted to zero between 0.9 nm and 1.2 nm to reduce cutoff noise. For electrostatic interactions, the Coulombic potential, with a cutoff of 1.2 nm, was smoothly shifted to zero from 0 to 1.2 nm. The relative dielectric constant was 15, which was the default value of the force field.<sup>28</sup> DPPC, water and NPs were coupled separately to Berendsen heat baths<sup>45</sup> at T, with a coupling constant  $\tau=1\text{ps}$ . The monolayer compression was simulated using semiisotropic pressure coupling (Berendsen coupling scheme,<sup>45</sup> coupling constant of 4 ps, compressibility in the lateral direction of  $5\times 10^{-5}\text{ bar}^{-1}$  and in the normal direction of zero). Each of the simulations was performed for 400 ns with a time step of 40 fs. The neighbor list for non-bonded interactions was updated every 10 steps. Snapshots of the simulation system in this paper were all

rendered by VMD.<sup>46</sup> All simulations were performed

with the GROMACS simulation package.<sup>47</sup>

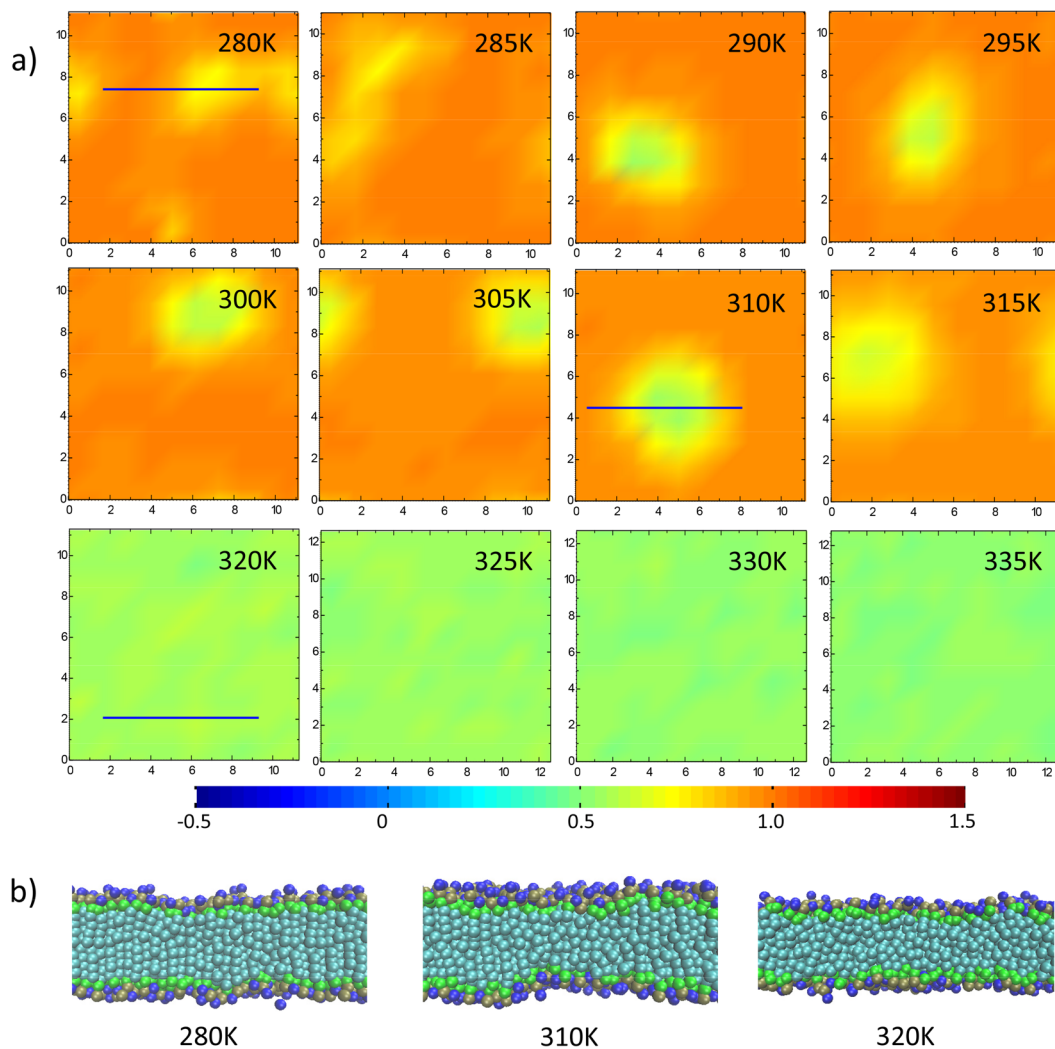


Figure 2. a) Two-dimensional (2D) phase map of pure DPPC bilayer during the gel-to-fluid phase transition, different colors correspond to different order parameters as shown in the color bar; b) Snapshots of section view of DPPC bilayer marked using blue line in a). DPPC bilayer experiences gel phase (280K), to ripple-like phase (290K), to fluid phase (320K).

### 3 Results and discussion

#### 3.1 Phase transition kinetics of the pure DPPC bilayer

The different phases of the pure DPPC bilayer have been studied by various experimental methods. It is known that the DPPC bilayer can exist in many phases such the fluid phase, the ripple phase, the gel phase, the subgel phase, the nonlamellar cubic phase, and the inverse hexagonal phase.<sup>30, 48, 49</sup> The transition from the ripple phase to the fluid phase is defined as the main phase transition. And the occurrence of the main phase transition is always accompanied by sudden shifts in parameters such as the volume, the

area per lipid, the lipid tail order parameter, which can be easily quantified both in experiments<sup>48, 49</sup> and simulations.<sup>29-32, 50</sup>

In order to capture the process of the main phase transition, the area per lipid (Figure 4) and the lipid order parameter (Figure 5) are calculated. After T=315K, the area per lipid experiences a sudden increase and the lipid order parameter obtained a sudden decrease, which characterize the occurrence of the main phase transition. Hence, we can get the main phase transition temperature ( $T_m$ ) of the pure DPPC bilayer as about  $T_m=315K$  from our simulations

results, which is similar to gel-to-fluid simulations reported by Rodgers *et al.*<sup>30</sup> It is worth mentioning that this value is quite different from  $295\pm 5$ K calculated by the developer of Martini force field.<sup>51</sup> By carefully comparing the differences between our simulation systems and relative systems, we can ascribe the difference between the results to mainly the system size together with the force field itself.  $295\pm 5$ K is the result from larger systems using the initial version of Martini force field,<sup>51, 52</sup> while 315K comes from smaller systems using improved Martini force field.<sup>28-30</sup> For comparison, we enlarge smaller systems to 4-fold systems (2048 DPPC molecules), and find the main phase transition temperature of the pure DPPC bilayer is reduced to 310K (Figure S4). But the trends of NP's effects are same both for the smaller and the larger systems, which validate our results of smaller systems.

We further calculate two dimensional (2D) phase map of the DPPC bilayer to capture the details. 2D

phase map is constructed using lipid order parameters of DPPC molecules as described in our previous work.<sup>36</sup> As shown in Figure 2a, 2D phase map clearly show the lipid tail order parameter of the DPPC bilayer at different temperature. At T=280K, the tail order parameters of all lipids are large representing consistent orientation of lipid tails, which corresponds to the gel phase. When increasing temperature to 290K, a liquid-disordered lipid nanodomain appears (green region in 290K-315K of Figure 2a). The snapshot (Figure 2b) further shows this is ripple-like phase, which is similar to "the intermediate phase" reported by Rodgers *et al.*<sup>30</sup> Then after 315K, the whole map is green corresponding lipid-disordered state and thus the fluid phase. Our simulation and analysis methods well reproduced the main phase transition of pure DPPC bilayer.

### 3.2 Phase transition temperature of the DPPC bilayer encapsulating hydrophobic NP

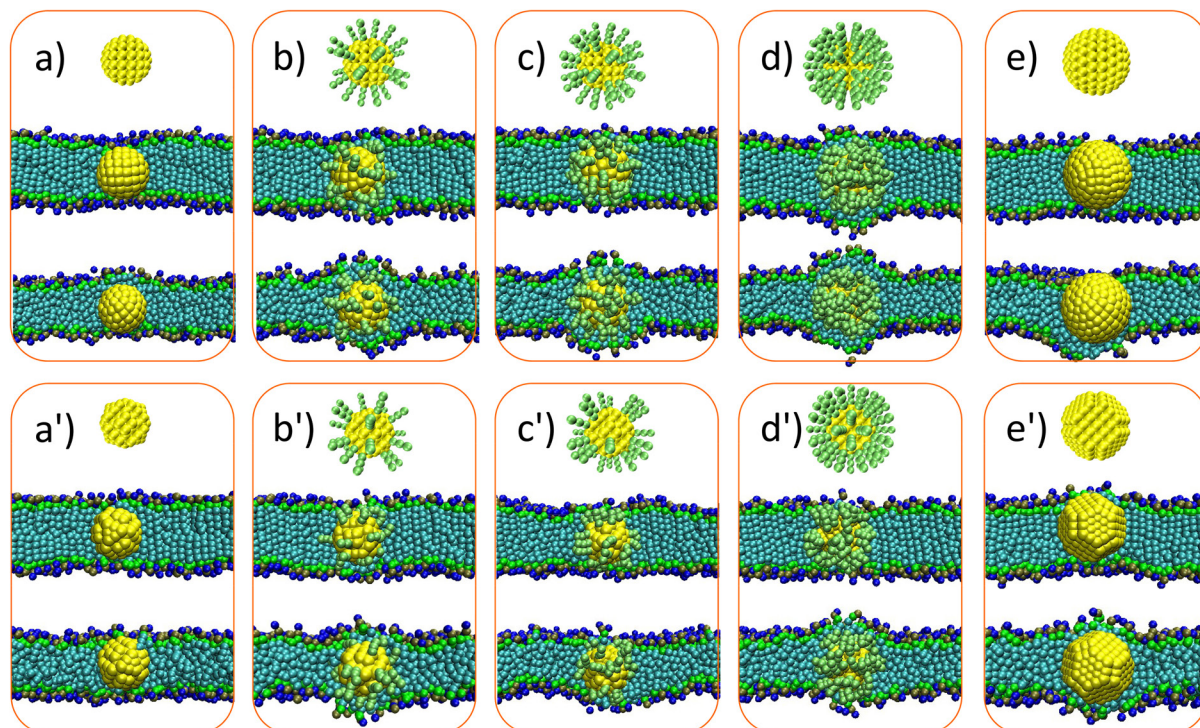


Figure 3. Snapshots of smooth NP of 3nm (0% ligands, a), 3nm (33%, b), 3nm (50%, c), 3nm (100%, d), 4nm (0%, e) and its encapsulation in the DPPC bilayer of gel phase (middle of orange box) and fluid phase (bottom of orange box). a'-e') are corresponding cases of rough NP similar to smooth NP. The color of DPPC and NPs are the same as Figure 1. Water molecules are not shown for clarity.

As has been reported, hydrophobic NP with size less than or comparable to the membrane thickness can be easily encapsulated into the lipid bilayer.<sup>10-12</sup> In the present work, our focus is the relationship

between the main phase transition temperature of DPPC bilayer and the surface properties of encapsulating NP rather than the penetration dynamic of different NPs. The latter is also widely

studied by many other researches.<sup>11, 34-44</sup> Hence, we just perform pulling simulation to drag NPs into the hydrophobic region of the DPPC bilayer at T=335K. All NPs can easily encapsulated into the DPPC bilayer and reside stably in the hydrophobic region of the bilayer along all the simulation time. Then the obtained NP-bilayer complex systems are cooled to T=280K as the initial systems for the main phase transition simulations.

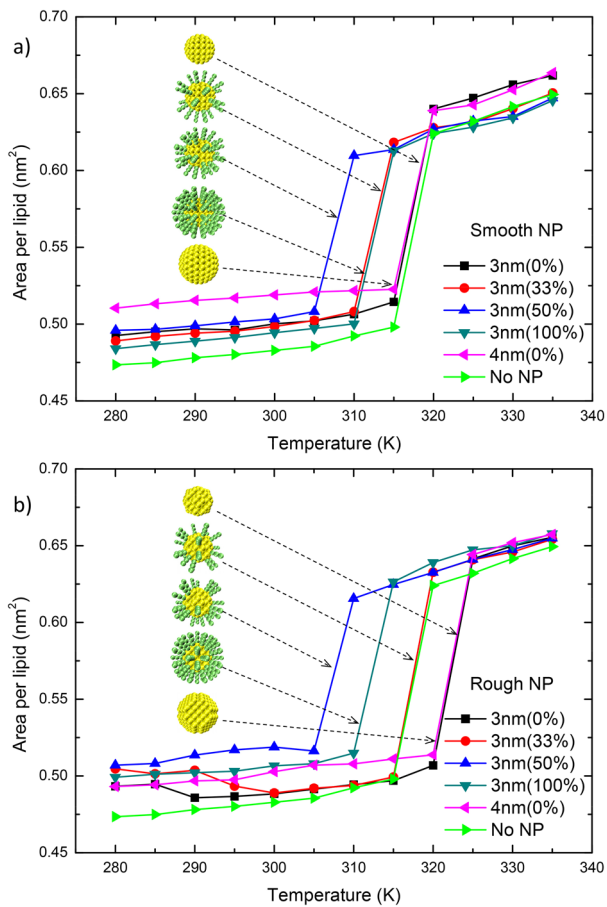


Figure 4. Variation of area per lipid during the main phase transition process for DPPC bilayer encapsulating smooth NP (a) and rough NP (b). Green line is for the case of pure DPPC bilayer.

With the encapsulation of hydrophobic NPs, the orientation of DPPC molecules adjacent to NPs are disrupted (Figure 3 and Figure S1), which is consistent with the reconstruction of neighboring DPPC molecules induced by NPs reported in the experiments of Wang *et al.*<sup>3</sup>. This disruption is similar at all temperatures considered in our simulations. Besides, no liquid-disordered lipid nanodomain far from NP exists before the main phase transition. This does not represent the disappearance of ripple-like

phase, since NP may prefer to interact with the fluid phase lipid bilayer rather than gel phase lipid bilayer.<sup>53</sup> In other words, the liquid-disordered lipid nanodomain may appear on the location of NP. In addition, it is worth mentioning that the disruption does not dominate the whole phase behavior at each specific temperature and all hydrophobic NPs can stably reside in the DPPC bilayer of both gel phase and fluid phase during the whole gel-to-fluid phase transition simulations (Figure S2, S3).

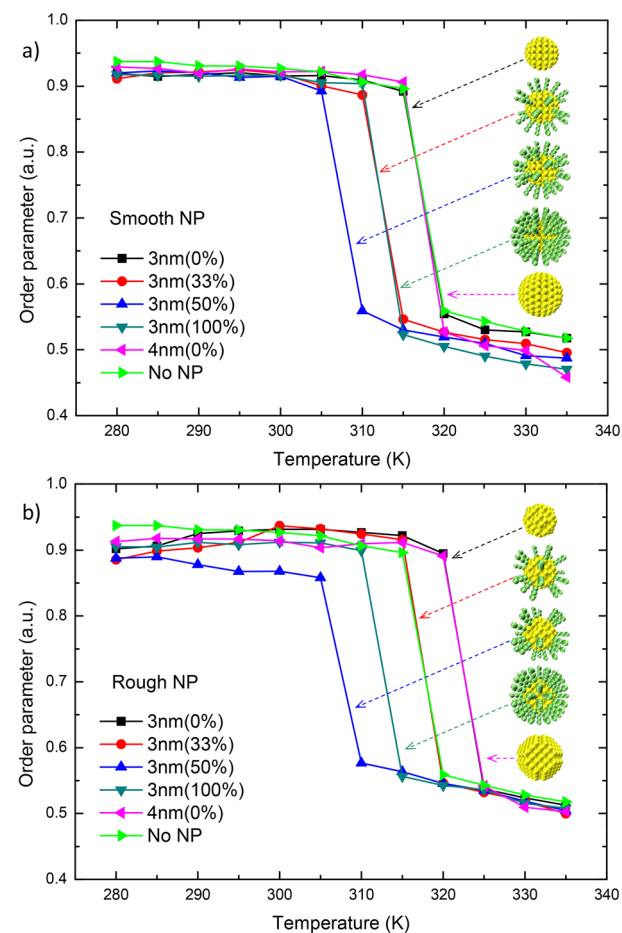


Figure 5. Variation of order parameter during the main phase transition process for DPPC bilayer encapsulating smooth NP (a) and rough NP (b). Green line is for the case of pure DPPC bilayer.

The area per lipid and the lipid tail order parameter are calculated to study the phase transition kinetics of the DPPC bilayer encapsulating NP (Figure 4, 5). Lipids of the fluid phase are characterized by larger area per lipid and smaller lipid tail order parameter compared with that of gel phase. The sudden increase of the area per lipid and the sudden decrease of lipid tail order parameter

correspond to the occurrence of the gel-to-fluid phase transition. In general, Figure 4 and Figure 5 show that the main phase transition temperature can be increased or decreased by encapsulating NPs with proper surface roughness and density of surface ligand molecules into the DPPC bilayer. Figure 6 further summarizes the effects of surface roughness and the density of ligand molecules on the main phase transition temperature of DPPC bilayer. For smooth NP, 3nm (0%) shows no effects on the  $T_m$ . With the increase of the density of ligand molecules (0%-100%),  $T_m$  firstly decreases to a low value and then increase slightly. 4nm (0%) also shows no little effects on the  $T_m$ , which can exclude the effects of size increase induced by ligand molecules. For rough NP, 3nm (0%) can increase  $T_m$ . And the effect of the density of ligand molecules is similar to that of smooth NP. With the increase of surface ligand molecules, the effects of NPs are gradually dominated by the ligand molecules (such as cases of 50% and 100%). The results are supported by some recent experimental studies on the effects of hydrophobic NPs on the main phase transition temperature of lipid bilayer.<sup>25,26</sup> For example, Bothun embedded Ag-decanethiol NPs into DPPC bilayer and further found the main phase transition temperature was reduced.<sup>25</sup> Decanethiol molecules are modified to the surface of Ag NPs via covalent interactions to form Ag-decanethiol NPs. And covalent interactions are strong enough to keep decanethiol molecules on the surface of Ag NPs while in the hydrophobic region of DPPC bilayer. Here, Ag NPs with enough surface molecules can bring down the main phase transition temperature of DPPC bilayer, which is consistent with our simulations. More recently, White *et al.* demonstrated the main phase transition temperature of DPPC/DPPG vesicles can be largely increased by encapsulating stearylamine (SA)-stabilized Au NPs.<sup>26</sup> SA molecules are attached to the surface of Au NPs due to electrostatic interactions. However, it is well documented that surface roughness has influence on the attachment and detachment of colloids on surfaces.<sup>54-56</sup> Hence, SA molecules may detach from the surface of NPs to form naked Au NPs in the hydrophobic region of DPPC/DPPG bilayer. The naked Au NPs, which have rougher surface, further increase the main phase transition temperature of

lipid bilayer together with the free SA molecules. The results of the FCC-stacked rough NP in our simulations are completely consistent with the behaviors of Au NPs mentioned above.

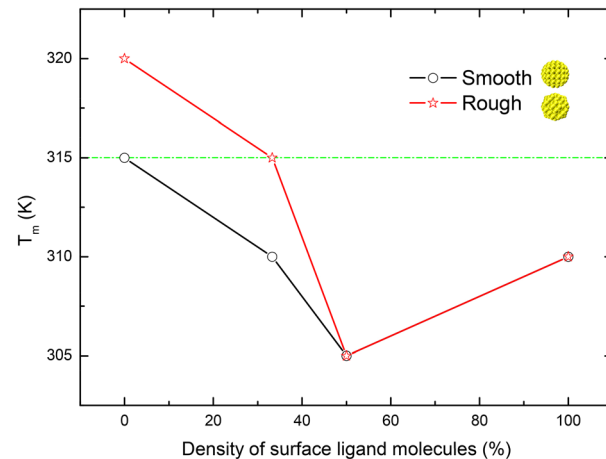


Figure 6. The relationship between the main phase transition temperature ( $T_m$ ) of DPPC bilayer and the surface properties of its encapsulating NPs. Green line (315K) is for the case of pure DPPC bilayer.

## 4 Conclusion

To summarize the findings presented in our study, we have performed coarse-grained molecular dynamics simulations to probe the effects of encapsulated NPs on the main phase transition temperature of DPPC bilayer. Results have shown that tuning the properties of NPs such as surface roughness and the density of ligand molecules can help modulate the main phase transition temperature of the DPPC bilayer. Increasing the surface roughness of NPs can raise the main phase transition temperature of DPPC bilayer, while increasing the density of surface ligand molecules of NPs can make the main phase transition temperature of DPPC bilayer firstly decrease and then increase. The results may provide insights for best design of hybrid NP-vesicle systems and thus promote their biomedical applications in drug release systems, etc.

## Acknowledgements

We acknowledge the support of this research from the National Important Basic Research Program of China (No. 2011CB933503), the National Natural Science Foundation of China (No. 61127002), the Basic Research Program of Jiangsu Province (No. BK2011036), and the Outstanding Ph.D. Student

Program of China's Ministry of Education.

**Electronic Supplementary Material:** Supplementary material (Details about Martini force field, two-dimensional phase maps of the DPPC bilayer encapsulating NP at different temperatures, system size effects.) is available in the online version of this article at [http://dx.doi.org/10.1007/s12274-\\*\\*\\*-\\*\\*\\*\\*-\\*](http://dx.doi.org/10.1007/s12274-***-****-*) (automatically inserted by the publisher).

## References

- [1] Al-Jamal, W.; Kostarelos, K. Liposome-nanoparticle hybrids for multimodal diagnostic and therapeutic applications. *Nanomedicine*, **2007**, *2*, 85-98.
- [2] Zhang, L.; Granick, S.. How to Stabilize Phospholipid Liposomes (Using Nanoparticles). *Nano Lett.*, **2006**, *6*, 694-698.
- [3] Wang, B.; Zhang, L.; Bae, S. C.; Granick, S. Nanoparticle-induced surface reconstruction of phospholipid membranes. *Proc. Natl. Acad. Sci. U.S.A.*, **2008**, *105*, 18171-18175.
- [4] Urban, A. S.; Fedoruk, M.; Horton, M. R.; Rädler, J. O.; Stefani, F. D.; Feldmann, J.. Controlled Nanometric Phase Transitions of Phospholipid Membranes by Plasmonic Heating of Single Gold Nanoparticles. *Nano Lett.*, **2009**, *9*, 2903-2908.
- [5] Chen, Y.; Bose, A.; Bothun, G. D. Controlled Release from Bilayer-Decorated Magnetoliposomes via Electromagnetic Heating. *ACS Nano*, **2010**, *4*, 3215-3221.
- [6] Amstad, E.; Kohlbrecher, J.; Müller, E.; Schweizer, T.; Textor, M.; Reimhult, E. Triggered Release from Liposomes through Magnetic Actuation of Iron Oxide Nanoparticle Containing Membranes. *Nano Lett.*, **2011**, *11*, 1664-1670.
- [7] An, X.; Zhan, F.; Zhu, Y. Smart Photothermal-Triggered Bilayer Phase Transition in AuNPs-Liposomes to Release Drug. *Langmuir*, **2013**, *29*, 1061-1068.
- [8] Gopalakrishnan, G.; Danelon, C.; Izewska, P.; Prummer, M.; Bolinger, P. Y.; Geissbühler, I.; Demurtas, D.; Dubochet, J.; Vogel, H. Multifunctional Lipid/Quantum Dot Hybrid Nanocontainers for Controlled Targeting of Live Cells. *Angew. Chem. Int. Ed.*, **2006**, *45*, 5478-5483.
- [9] Marshall, J. D.; Schnitzer, M. J. Optical Strategies for Sensing Neuronal Voltage Using Quantum Dots and Other Semiconductor Nanocrystals. *ACS Nano*, **2013**, *7*, 4601-4609.
- [10] Qiao, R.; Roberts, A. P.; Mount, A. S.; Klaine, S. J.; Ke, P. C. Translocation of C60 and Its Derivatives Across a Lipid Bilayer. *Nano Lett.*, **2007**, *7*, 614-619.
- [11] Lin, X.; Li, Y.; Gu, N. Nanoparticle's size effect on its translocation across a lipid bilayer: A molecular dynamics simulation. *J. Comput. Theor. Nanosci.*, **2010**, *7*, 269-276.
- [12] Ginzburg, V. V.; Balijepalli, S. Modeling the Thermodynamics of the Interaction of Nanoparticles with Cell Membranes. *Nano Lett.*, **2007**, *7*, 3716-3722.
- [13] Nangia, S.; Sureshkumar, R. Effects of Nanoparticle Charge and Shape Anisotropy on Translocation through Cell Membranes. *Langmuir*, **2012**, *28*, 17666-17671.
- [14] Wang, H.; Michielssens, S.; Moors, S. L. C.; Ceulemans, A. Molecular Dynamics Study of Dipalmitoylphosphatidylcholine Lipid Layer Self-Assembly onto a Single-Walled Carbon Nanotube. *Nano Res.*, **2009**, *2*, 945-954.
- [15] Lehn, R. C. V.; Atukorale, P. U.; Carney, R. P.; Yang, Y. S.; Stellacci, F.; Irvine, D. J.; Alexander-Katz, A. Effect of Particle Diameter and Surface Composition on the Spontaneous Fusion of Monolayer-Protected Gold Nanoparticles with Lipid Bilayers. *Nano Lett.*, **2013**, *13*, 4060-4067.
- [16] Grzelczak, M.; Perez-Juste, J.; Mulvaney, P.; Liz-Marzan, L. M. Shape control in gold nanoparticle synthesis. *Chem. Soc. Rev.*, **2008**, *37*, 1783-1791.
- [17] Alkilany, A. M.; Lohse, S. E.; Murphy, C. J. The Gold Standard: Gold Nanoparticle Libraries To Understand the Nano-Bio Interface. *Acc. Chem. Res.*, **2013**, *46*, 650-661.
- [18] Sun, Y. Controlled synthesis of colloidal silver nanoparticles inorganic solutions: empirical rules for nucleation engineering. *Chem. Soc. Rev.*, **2013**, *42*, 2497-2511.
- [19] Kim, S. T.; Saha, K.; Kim, C.; Rotello, V. M. The Role of Surface Functionality in Determining Nanoparticle Cytotoxicity. *Acc. Chem. Res.*, **2013**, *46*, 681-691.
- [20] Rasch, M. R.; Rossinyol, E.; Hueso, J. L.; Goodfellow, B. W.; Arbiol, J.; Korgel, B. A. Hydrophobic Gold Nanoparticle Self-Assembly with Phosphatidylcholine Lipid: Membrane-Loaded and Janus Vesicles. *Nano Lett.*, **2010**, *10*, 3733-3739.
- [21] Rasch, M. R.; Yu, Y.; Bosoy, C.; Goodfellow, B. W.; Korgel, B. A. Chloroform-Enhanced Incorporation of Hydrophobic Gold Nanocrystals into Dioleoylphosphatidylcholine (DOPC) Vesicle Membranes. *Langmuir*, **2012**, *28*, 12971-12981.
- [22] Lee, H. Y.; Shin, S. H. R.; Abezgauz, L. L.; Lewis, S. A.; Chirsan, A. M.; Danino, D. D.; Bishop, K. J. M. Integration of Gold Nanoparticles into Bilayer Structures via Adaptive Surface Chemistry. *J. Am. Chem. Soc.*, **2013**, *135*, 5950-5953.
- [23] Park, S. H.; Oh, S. G.; Mun, J. Y.; Han, S. S. Effects of silver nanoparticles on the fluidity of bilayer in phospholipid liposome. *Colloid Surf. B-Biointerfaces*, **2005**, *44*, 117-122.
- [24] Park, S. H.; Oh, S. G.; Mun, J. Y.; Han, S. S. Loading of gold nanoparticles inside the DPPC bilayers of liposome and their effects on membrane fluidities. *Colloid Surf. B-Biointerfaces*, **2006**, *48*, 112-118.
- [25] Bothun, G. D. Hydrophobic silver nanoparticles trapped in lipid bilayers: Size distribution, bilayer phase behavior, and optical properties. *J. Nanobiotechnol.*, **2008**, *6*, 13/1-10.
- [26] White, G. V.; Chen, Y.; Roder-Hanna, J.; Bothun, G. D.; Kitchens, C. L. Structural and Thermal Analysis of Lipid Vesicles Encapsulating Hydrophobic Gold Nanoparticles. *ACS Nano*, **2012**, *6*, 4678-4685.
- [27] Nagle, J. F. Theory of the Main Lipid Bilayer Phase Transition. *Ann. Rev. Phys. Chem.*, **1980**, *31*, 157-195.
- [28] Marrink, S. J.; Risselada, H. J.; Yefimov, S.; Tieleman, D. P.; de Vries, A. H. The MARTINI Force Field: Coarse Grained Model for Biomolecular Simulations. *J. Phys. Chem. B*, **2007**, *111*, 7812-7824.

- [29] Ramalho, J. P. P.; Gkeka, P.; Sarkisov, L. Structure and Phase Transformations of DPPC Lipid Bilayers in the Presence of Nanoparticles: Insights from Coarse-Grained Molecular Dynamics Simulations. *Langmuir*, **2011**, *27*, 3723-3730.
- [30] Rodgers, J. M.; Sørensen, J.; de Meyer, F. J. M.; Schiøtt, B.; Smit, B. Understanding the Phase Behavior of Coarse-Grained Model Lipid Bilayers through Computational Calorimetry. *J. Phys. Chem. B*, **2012**, *116*, 1551-1569.
- [31] Hakobyan, D.; Heuer, A. Phase Separation in a Lipid/Cholesterol System: Comparison of Coarse-Grained and United-Atom Simulations. *J. Phys. Chem. B*, **2013**, *117*, 3841-3851.
- [32] Waheed, Q.; Tjörnhammar, R.; Edholm, O. Phase Transitions in Coarse-Grained Lipid Bilayers Containing Cholesterol by Molecular Dynamics Simulations. *Biophys. J.*, **2012**, *103*, 2125-2133.
- [33] Marrink, S. J.; Tieleman, D. P. Perspective on the Martini model. *Chem. Soc. Rev.*, **2013**, *42*, 6801-6822.
- [34] Li, Y.; Chen, X.; Gu, N. Computational Investigation of Interaction between Nanoparticles and Membranes: Hydrophobic/Hydrophilic Effect. *J. Phys. Chem. B*, **2008**, *112*, 16647-16653.
- [35] Li, Y.; Gu, N. Thermodynamics of Charged Nanoparticle Adsorption on Charge-Neutral Membranes: A Simulation Study. *J. Phys. Chem. B*, **2010**, *114*, 2749-2754.
- [36] Lin, X.; Wang, C.; Wang, M.; Fang, K.; Gu, N. Computer Simulation of the Effects of Nanoparticles' Adsorption on the Properties of Supported Lipid Bilayer. *J. Phys. Chem. C*, **2012**, *116*, 17960-17968.
- [37] Vácha, R.; Martinez-Veracoechea, F. J.; Frenkel, D. Receptor-Mediated Endocytosis of Nanoparticles of Various Shapes. *Nano Lett.*, **2011**, *11*, 5391-5395.
- [38] Vácha, R.; Martinez-Veracoechea, F. J.; Frenkel, D. Intracellular Release of Endocytosed Nanoparticles Upon a Change of Ligand-Receptor Interaction. *ACS Nano*, **2012**, *6*, 10598-10605.
- [39] Yue, T.; Zhang, X. Cooperative Effect in Receptor-Mediated Endocytosis of Multiple Nanoparticles. *ACS Nano*, **2012**, *6*, 3196-3205.
- [40] Li, Y.; Yue, T.; Yang, K.; Zhang, X. Molecular modeling of the relationship between nanoparticle shape anisotropy and endocytosis kinetics. *Biomaterials*, **2012**, *33*, 4965-4973.
- [41] Huang, C.; Zhang, Y.; Yuan, H.; Gao, H.; Zhang, S. Role of Nanoparticle Geometry in Endocytosis: Laying Down to Stand Up. *Nano Lett.*, **2013**, *13*, 4546-4550.
- [42] Yang, K.; Ma, Y. Q. Computer simulation of the translocation of nanoparticles with different shapes across a lipid bilayer. *Nat. Nanotechnol.*, **2010**, *5*, 579-583.
- [43] Ding, H. M.; Tian, W. D.; Ma, Y. Q. Designing Nanoparticle Translocation through Membranes by Computer Simulations. *ACS Nano*, **2012**, *6*, 1230-1238.
- [44] Ding, H. M.; Ma, Y. Q. Controlling Cellular Uptake of Nanoparticles with pH-Sensitive Polymers. *Sci. Rep.*, **2013**, *3*, 2804/1-6.
- [45] Berendsen, H. J. C.; Postma, J. P. M.; van Gunsteren, W. F.; DiNola, A.; Haak, J. R. Molecular dynamics with coupling to an external bath. *J. Chem. Phys.*, **1984**, *81*, 3684-3690.
- [46] Humphrey, W.; Dalke, A.; Schulten, K. VMD: Visual Molecular Dynamics. *J. Mol. Graph.*, **1996**, *14*, 33-38.
- [47] Hess, B.; Kutzner, C.; van der Spoel, D.; Lindahl, E. GROMACS 4: Algorithms for Highly Efficient, Load-Balanced, and Scalable Molecular Simulation. *J. Chem. Theory Comput.*, **2008**, *4*, 435-447.
- [48] Koynova, R.; Caffrey, M. Phases and phase transitions of the phosphatidylcholines. *Biochim. Biophys. Acta*, **1998**, *1376*, 91-145.
- [49] Nagle, J. F.; Tristram-Nagle, S. Structure of lipid bilayers. *Biochim. Biophys. Acta*, **2000**, *1469*, 159-195.
- [50] Kong, X.; Qin, S.; Lu, D.; Liu, Z. Surface tension effects on the phase transition of a DPPC bilayer with and without protein: a molecular dynamics simulation. *Phys. Chem. Chem. Phys.*, **2014**, *16*, 8434-8440.
- [51] Marrink, S. J.; Risselada, J.; Mark, A. E. Simulation of gel phase formation and melting in lipid bilayers using a coarse grained model. *Chem. Phys. Lipids*, **2005**, *135*, 223-244.
- [52] Marrink, S. J.; de Vries, A. H.; Mark, A. E. Coarse Grained Model for Semiquantitative Lipid Simulations. *J. Phys. Chem. B*, **2004**, *108*, 750-760.
- [53] Mecke, A.; Majoros, I. J.; Patri, A. K.; Baker, Jr. J. R.; Holl, M. M. B.; Orr, B. G. Lipid Bilayer Disruption by Polycationic Polymers: The Roles of Size and Chemical Functional Group. *Langmuir*, **2005**, *21*, 10348-10354.
- [54] Shen, C.; Lazouskaya, V.; Zhang, H.; Wang, F.; Li, B.; Jin, Y.; Huang, Y. Theoretical and experimental investigation of detachment of colloids from rough collector surfaces. *Colloid Surf. A-Physicochem. Eng. Asp.*, **2012**, *410*, 98-110.
- [55] Shen, C.; Wang, F.; Li, B.; Jin, Y.; Wang, L.; Huang, Y. Application of DLVO Energy Map To Evaluate Interactions between Spherical Colloids and Rough Surfaces. *Langmuir*, **2012**, *28*, 14681-14692.
- [56] Shen, C.; Lazouskaya, V.; Zhang, H.; Li, B.; Jin, Y.; Huang, Y. Influence of surface chemical heterogeneity on attachment and detachment of microparticles. *Colloid Surf. A-Physicochem. Eng. Asp.*, **2013**, *433*, 14-29.

## Electronic Supplementary Material

# Possible Mechanism for Regulating the Main Phase Transition Temperature of Lipid Bilayers via Hydrophobic Nanoparticles: A Simulation Study

Xubo Lin, Ning Gu (✉)

*State Key Laboratory of Bioelectronics and Jiangsu Key Laboratory for Biomaterials and Devices, School of Biological Science & Medical Engineering, Southeast University, Nanjing, 210096, People's Republic of China*

Supporting information to DOI 10.1007/s12274-\*\*\*\*-\*\*\*\*-\* (automatically inserted by the publisher)

### Details about Martini force field

Table 1. The interaction level between different CG bead types

sub	Q				P					N				C				
	da	d	a	0	5	4	3	2	1	da	d	a	0	5	4	3	2	1
Q	da	O	O	II	O	O	O	I	I	I	I	I	IV	V	VI	VII	IX	IX
	d	O	I	O	II	O	O	I	I	I	III	I	IV	V	V	VII	IX	IX
	a	O	O	I	II	O	O	I	I	I	I	III	IV	V	VI	VII	IX	IX
	0	II	II	II	IV	I	O	I	II	III	III	III	IV	V	VI	VII	IX	IX
P	5	O	O	O	I	O	O	O	O	I	I	I	IV	V	VI	VI	VII	VIII
	4	O	O	O	O	O	I	I	II	II	III	III	IV	V	VI	VI	VII	VIII
	3	O	O	O	I	O	I	I	II	II	II	II	IV	IV	V	VI	VII	VII
	2	I	I	I	II	O	II	II	II	II	II	II	IV	IV	V	VI	VII	VII
	1	I	I	I	III	O	II	II	II	II	II	II	IV	IV	IV	V	VI	VI
N	da	I	I	I	III	I	III	II	II	II	II	II	IV	V	VI	VI	VI	VI
	d	I	III	I	III	I	III	II	II	II	II	II	IV	IV	V	VI	VI	VI
	a	I	I	III	III	I	III	II	II	II	II	III	IV	IV	V	VI	VI	VI
	0	IV	IV	IV	IV	IV	IV	IV	III	III	IV	IV	IV	IV	IV	IV	V	VI
C	5	V	V	V	V	V	IV	IV	IV	IV	IV	IV	IV	IV	IV	IV	V	V
	4	VI	VI	VI	VI	VI	V	IV	IV	V	V	V	IV	IV	IV	IV	V	V
	3	VII	VII	VII	VII	VI	VI	V	IV	VI	VI	VI	IV	IV	IV	IV	IV	IV
	2	IX	IX	IX	IX	VII	VII	VI	VI	V	VI	VI	V	V	V	IV	IV	IV
	1	IX	IX	IX	IX	VIII	VIII	VII	VII	VI	VI	VI	V	V	IV	IV	IV	IV

Level of interaction indicates the well depth in the LJ potential: O,  $\varepsilon = 5.6$  kJ/mol; I,  $\varepsilon = 5.0$  kJ/mol; II,  $\varepsilon = 4.5$  kJ/mol; III,  $\varepsilon = 4.0$  kJ/mol; IV,  $\varepsilon = 3.5$  kJ/mol; V,  $\varepsilon = 3.1$  kJ/mol; VI,  $\varepsilon = 2.7$  kJ/mol; VII,  $\varepsilon = 2.3$  kJ/mol; VIII,  $\varepsilon = 2.0$  kJ/mol; IX,  $\varepsilon = 4.5$  kJ/mol. The LJ parameter  $\sigma = 0.47$  nm for all interaction levels except level IX for which  $\sigma = 0.62$  nm. Four different CG sites are considered: charged (Q), polar (P), nonpolar (N), and apolar (C). Subscripts are used to further distinguish groups with different chemical nature: 0, no hydrogen-bonding capabilities are present; d, groups acting as hydrogen bond donor; a, groups acting as hydrogen bond acceptor; da, groups with donor and acceptor options; 1-5, indicating increasing polar affinity. (Marrink, S. J.; Risselada, H. J.; Yefimov, S.; Tieleman, D. P.; de Vries, A. H. The MARTINI Force Field: Coarse Grained Model for Biomolecular Simulations. *J. Phys. Chem. B*, 2007, 111, 7812-7824.)

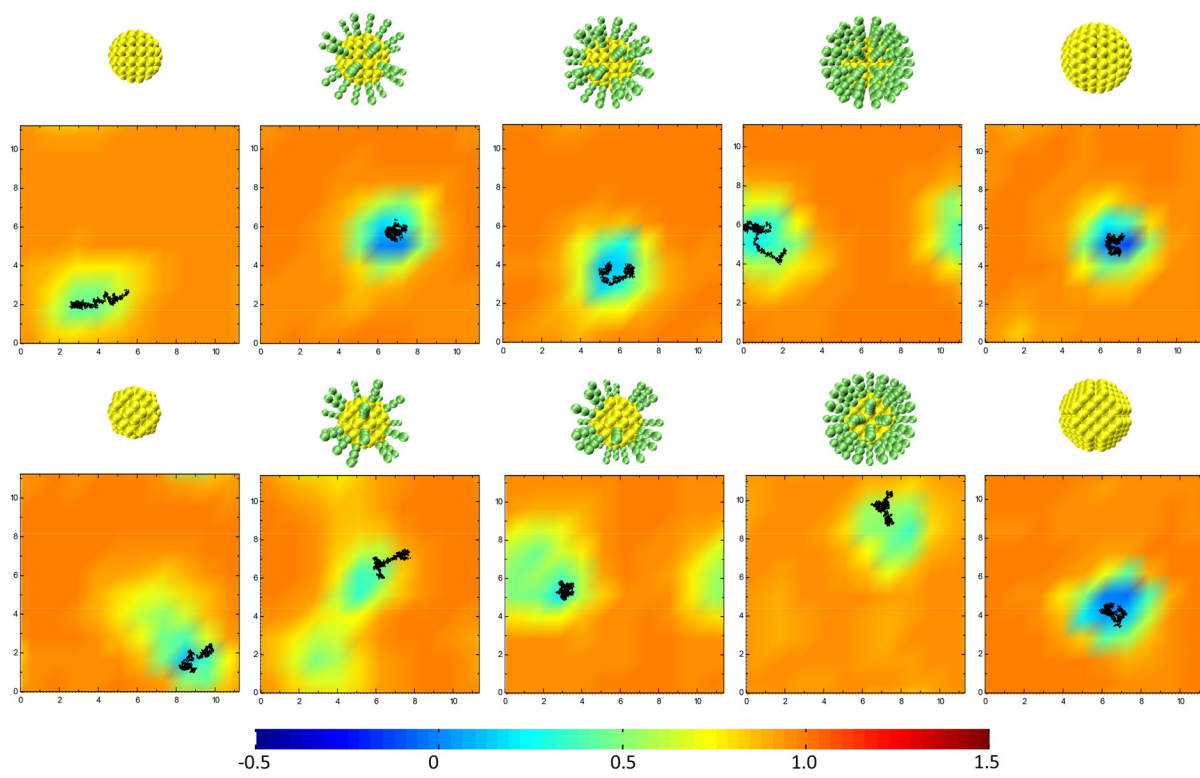


Figure S1. The phase behavior of DPPC bilayer encapsulating NPs at the initial state (280K) of phase transition simulations. Different colors correspond to different order parameters as shown in the color bar. Black line corresponds to the trajectory of NPs projected in the x-y plane.

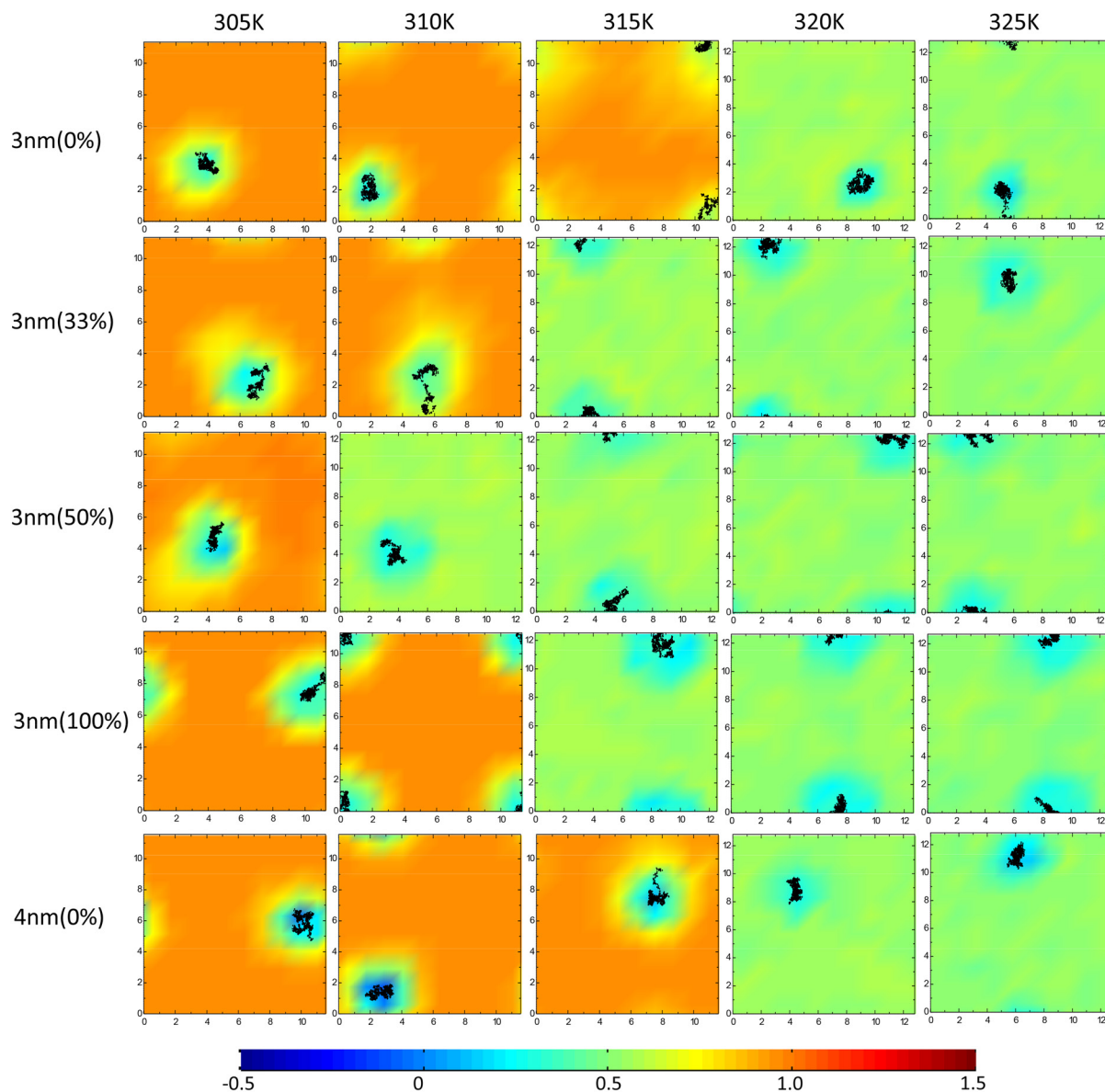


Figure S2. 2D phase map of DPPC bilayer encapsulating smooth NP for characterizing the gel-to-fluid phase transition. Different colors correspond to different order parameters as shown in the color bar. Black line corresponds to the trajectory of NPs projected in the x-y plane.

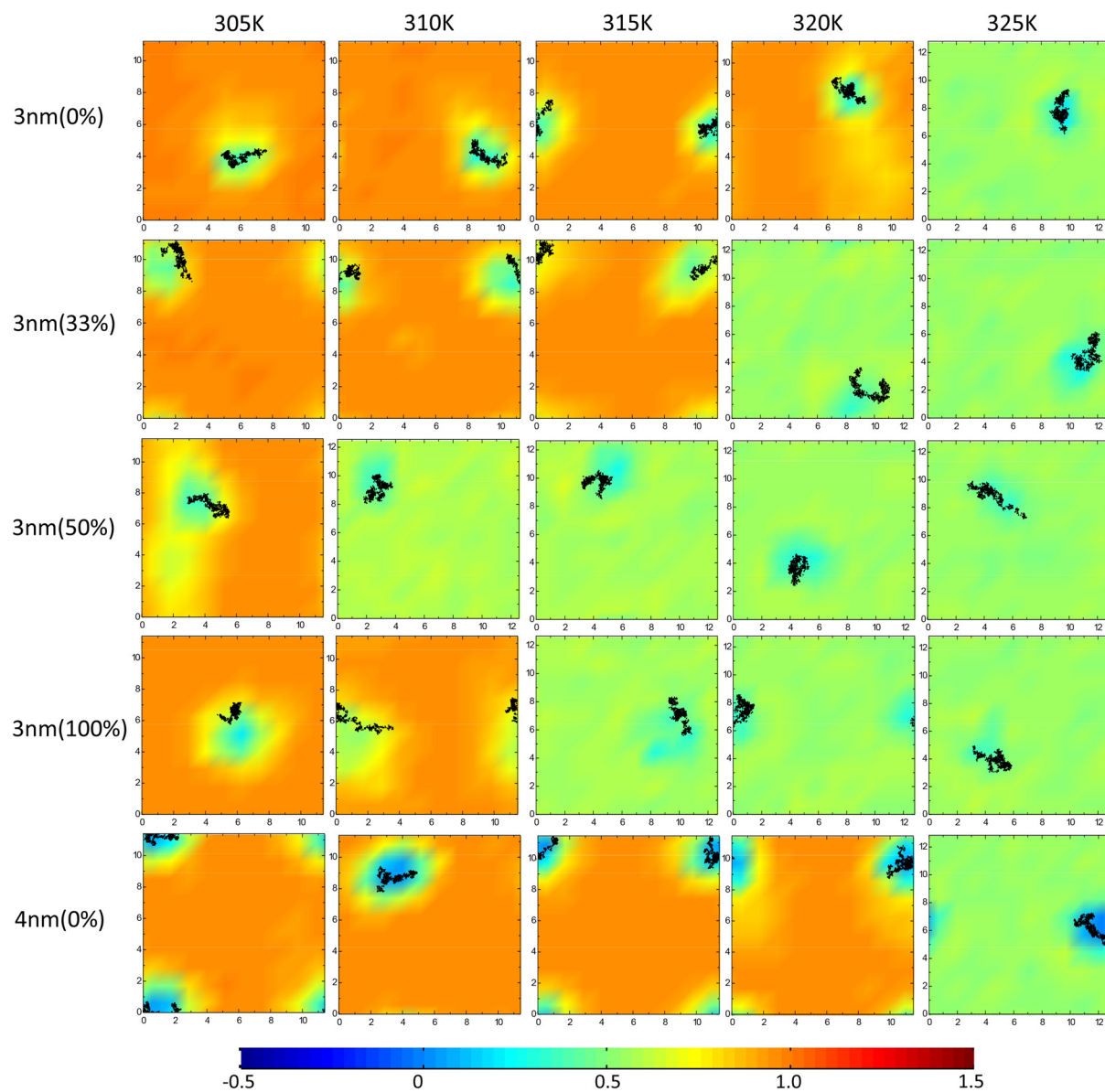


Figure S3. 2D phase map of DPPC bilayer encapsulating rough NP for characterizing the gel-to-fluid phase transition. Different colors correspond to different order parameters as shown in the color bar. Black line corresponds to the trajectory of NPs projected in the x-y plane.

## System Size Effects

In order to evaluate the system size effects on the phase behavior of the DPPC bilayer with or without NP, we expand the systems of 4nm (0%, rough), 4nm (0%, smooth), pure bilayer to 4-fold sizes (2048 DPPC molecules, 4 NPs, 70064 water molecules, Figure S4 a and b). The temperatures of the new systems are increased from 280K to 335K as described in the model and simulation details of the manuscript. As shown in Figure S4 c, the main phase transition temperature of the pure DPPC bilayer is reduced to 310K (not 315K described in the manuscript), which can be ascribed to more fluctuations of large systems. But the trends of the phase behavior of the DPPC bilayer encapsulating NPs are well reproduced as that of smaller systems described in manuscript: 4nm (0%, rough) could increase the main phase transition temperature, while 4nm (0%, smooth) show no effects on the main phase transition temperature. In other words, the results of the phase behavior of the smaller DPPC bilayer encapsulating NPs from coarse-grained molecular dynamics simulations in the manuscript should not be finite size effects.

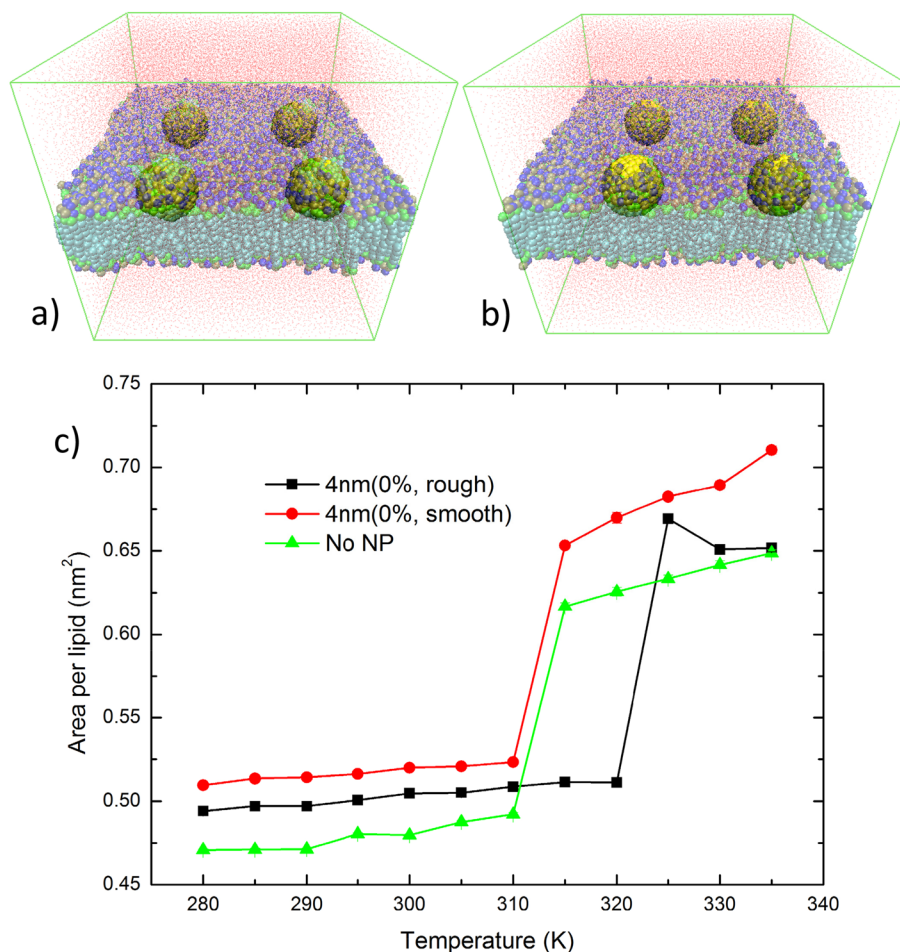


Figure S4. Side view of the 4-fold systems of 4nm (0%, rough) (a) and 4nm (0%, smooth) (b); Variation of area per lipid during the main phase transition process for DPPC bilayer encapsulating rough NP and smooth NP. Green line is for the case of pure DPPC bilayer.